3D Nano- and Micro-Manufacturing:

Technology and Technical Application

REGISTER NOW!

April 3 – 8, 2022 I Schöntal Monastery, Germany

Energy Level Alignment at the C_{60}/Monolayer-WS$_2$ Interface on Insulating and Conductive Substrates

Jie Ma, Patrick Amsalem, Thorsten Schultz, Dongguen Shin, Xiaomin Xu, and Norbert Koch*

Combining a transition metal dichalcogenide monolayer (ML) and molecular semiconductors is an attractive route for forming nanoscale hybrid van der Waals heterostructures with potentially novel (opto-)electronic properties. The energy level alignment at the hybrid interface governs these properties, but precise determination of the interfacial electronic structure is challenging due to the pronounced excitonic nature of both components and the non-trivial band structure of the inorganic ML. For instance, dielectric screening by the supporting substrate of such a heterostructure may impact the energy levels, but very few experiments have attended to this important issue to date. Here, it is shown how photoelectron spectroscopy can be used to unravel the energy level line-up at the C_{60}/ML-WS$_2$ interface supported on an insulating (sapphire) and a semi-metallic (graphite) substrates. On both substrates, an almost identical staggered type-II level alignment is determined. However, C_{60}/ML-WS$_2$ exhibits stronger n-type characteristics on sapphire, which is suggested to be due to native donor-type defects of ML-WS$_2$. While these remain occupied and active on the insulating substrate, they are emptied into the charge reservoir of the conductive substrate. These insights should be considered in the future design of functional heterostructures of inorganic ML and molecular semiconductor materials.

1. Introduction

2D materials are a steadily growing subject of research, involving multiple disciplines and spanning from fundamental investigations to novel device applications,[1–4] for example, thin-film transistors,[5–7] chemical sensors,[8] photodetectors,[9,10] and photovoltaic cells.[11–13] Unlike graphene with semi-metallic electronic properties,[14] 2D transition metal dichalcogenides (TMDCs) with chemical composition MX$_2$ (e.g., with M = Mo, W and X = S, Se) can feature a finite bandgap, rendering them semiconductors with unique structural,[15] (opto-)electronic,[16–18] and magnetic properties.[19,20] Remarkable features of TMDCs associated with their decreased dimensionality include, amongst others, valley polarization,[21] phase-stability of a monolayer (ML), emergence of a direct bandgap,[22,23] and large exciton binding energies.[24] Furthermore, TMDCs are comparably chemically inert and exhibit no dangling bonds, particularly in ML form.[25,26] This provides the opportunity for the fabrication of van der Waals heterostructures with molecular and organic semiconductors, which predominantly feature closed electronic shells. Such hybrid structures could combine the advantages of the two individual material classes, for example, the high charge carrier mobility of the TMDC ML and strong light-matter coupling across a wide energy range of the molecular compound.[25,27,28] Such molecular semiconductor/ML-TMDC heterostructures can feature advanced optoelectronic properties,[29,30] and these naturally depend strongly on the electronic properties of the interface. It is, therefore, crucially important to understand how the energy levels at such interfaces align, and how they can eventually be controlled. In this context, the reduced dimensionality of an ML-TMDC, being only three atoms thick, introduces an

J. Ma, Dr. P. Amsalem, Dr. T. Schultz, Dr. D. Shin, Prof. N. Koch
Institut für Physik & IRIS Adlershof
Humboldt-Universität zu Berlin
12489 Berlin, Germany
E-mail: norbert.koch@physik.hu-berlin.de

The ORCID identification number(s) for the author(s) of this article can be found under https://doi.org/10.1002/aelm.202100425.

J. Ma, Dr. T. Schultz, Prof. N. Koch
Helmholtz-Zentrum Berlin für Materialien und Energie GmbH
12489 Berlin, Germany

Prof. X. Xu
Institute of Materials Research
Tsinghua Shenzhen International Graduate School
Tsinghua University
Shenzhen 518055, China

Prof. X. Xu
Shenzhen Geim Graphene Center
Tsinghua-Berkeley Shenzhen Institute
Tsinghua University
Shenzhen 518055, China
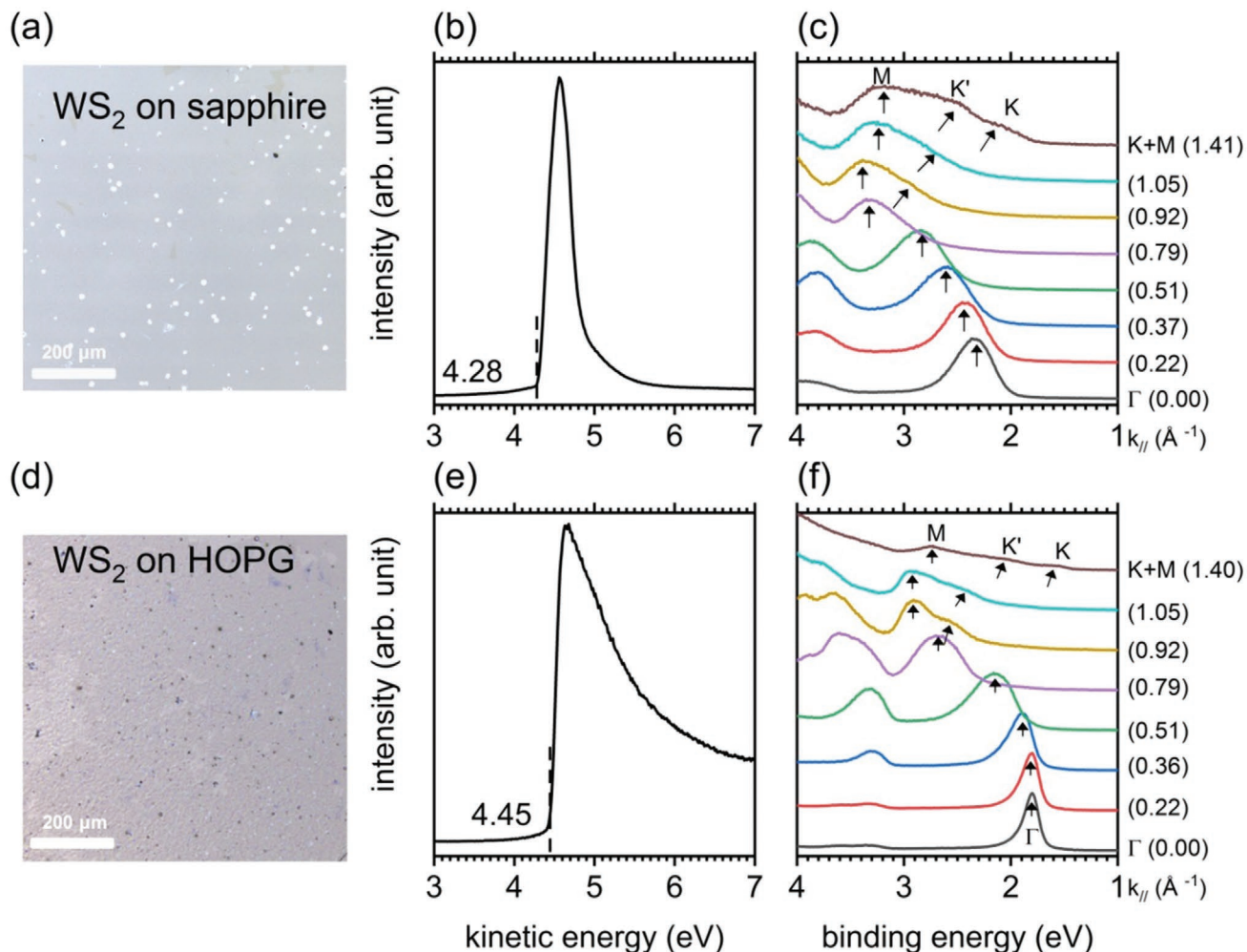
Figure 1. a,d) Optical microscope images of high-coverage WS$_2$ MLs on sapphire and HOPG. b,c) SECO and ARUPS spectra of ML WS$_2$ on sapphire. e,f) SECO and ARUPS spectra of ML WS$_2$ on HOPG. The arrows are guides for the band dispersion.

aspect in material properties that is not relevant when dealing with interfaces of 3D bulk materials. The electronic structure of ML-TMDCs depends on the dielectric environment, such as a supporting substrate,[31] leading to band gap and exciton energy renormalization.[32–34] Therefore, the dielectric constant (ε) of the substrate used for a molecule/ML-TMDC heterostructure is expected to impact its electronic properties and energy level alignment. Depending on the targeted functionality or device-implementation of a molecule/ML-TMDC structure, very different substrates can be relevant, ranging from the often low ε of insulators to the highest possible one of metals. Knowledge of the molecule/ML-TMDC interface electronic properties is needed for guiding device design, but only very few systems have been studied to date, particularly on insulating substrates. A major challenge in this framework is that the primary method to directly access electronic energy levels, that is, photoelectron spectroscopy, requires sufficient sample conductivity to avoid detrimental charging due to photoelectron emission. A metal or semi-metal substrate usually averts this problem, but a single layer TMDC on an insulating substrate calls for particular attention in experiments. The individual crystal flakes

forming a typical ML-TMDC sample must form sufficient percolation paths for lateral current flow across the entire sample to enable reliable determination of the electronic levels, as demonstrated only rather recently.[35,36] The same approach was adopted in the present study, by optimizing the chemical vapor deposition (CVD) growth conditions so that a quasi-continuous ML-WS$_2$ layer of coalesced crystal flakes formed on a macroscopic scale (see **Figure 1**). This warrants sufficient lateral conductivity within the ML-WS$_2$ layer for reliable photoelectron spectroscopy measurements.

Here, we investigate the electronic properties of a prototypical molecule/ML-TMDC combination, that is, C$_{60}$ deposited on ML-WS$_2$, and compare the energy level alignment for two different supporting substrates, that is, semi-metallic highly oriented pyrolytic graphite (HOPG) and insulating c-sapphire. To that end, we employ X-ray and angle-resolved ultraviolet photoelectron spectroscopy (XPS and ARUPS), the latter to access the global valence band maximum (VBM) of ML-WS$_2$ at the K-point of its Brillouin zone (BZ). The two substrates were chosen because the electronic properties of HOPG resemble those of graphene,[37] a promising electrode for nano-electronic

**ADVANCED
SCIENCE NEWS**
www.advancedsciencenews.com

**ADVANCED
ELECTRONIC
MATERIALS**
www.advelectronicmat.de

devices,[38,39] and because sapphire features transparency in the visible and near-infrared, thus often used in optical experiments. Both HOPG and sapphire have anisotropic but on-average similar dielectric constant values of about 10.[40,41] Therefore, the electronic properties of ML-WS$_2$ are expected to be comparable on both substrates, but experimental verification is not yet available. In contrast, the two substrates differ significantly in their electrical properties, and the influence of native WS$_2$ defects, that is, sulfur-vacancies,[42,43] and their possible interplay with a supporting substrate, on the electronic properties of the ML and its energy level alignment with a molecular semiconductor remains elusive to date. Fullerenes and their derivatives are prominent molecular semiconductors, widely employed in molecular-based optoelectronic devices.[44,45] Notably, bulk MoS$_2$-C$_{60}$ layered crystals (alternating layers of MoS$_2$ and C$_{60}$), which have been reported more than fifteen years ago, have been suggested to have potential for use in photovoltaic cells.[46] More recently, theoretical work proposed that the combination of WS$_2$ and C$_{60}$ should be more efficient for exciton dissociation compared to the MoS$_2$-C$_{60}$ pair.[13] Still, very few experimental investigations of the electronic properties of ML-TMDCs combined with C$_{60}$ and its derivatives have been reported so far,[46–48] and the supporting substrate was not yet considered an important parameter. To contribute towards an improved understanding of such hybrid systems, we carefully evaluate the electronic band line-up at the C$_{60}$/ML-WS$_2$ interface depending on the substrate. We find that indeed a van der Waals heterostructure with weak physisorptive interaction is formed, and interfacial vacuum level alignment prevails. On both substrates, a staggered type-II heterojunction suitable for charge separation results, with the C$_{60}$ frontier occupied levels ca. 0.4 eV below the ML-WS$_2$ VBM and confirming from an energy level alignment point of view the potential of this materials' pair for the fabrication of hybrid excitonic solar cells.
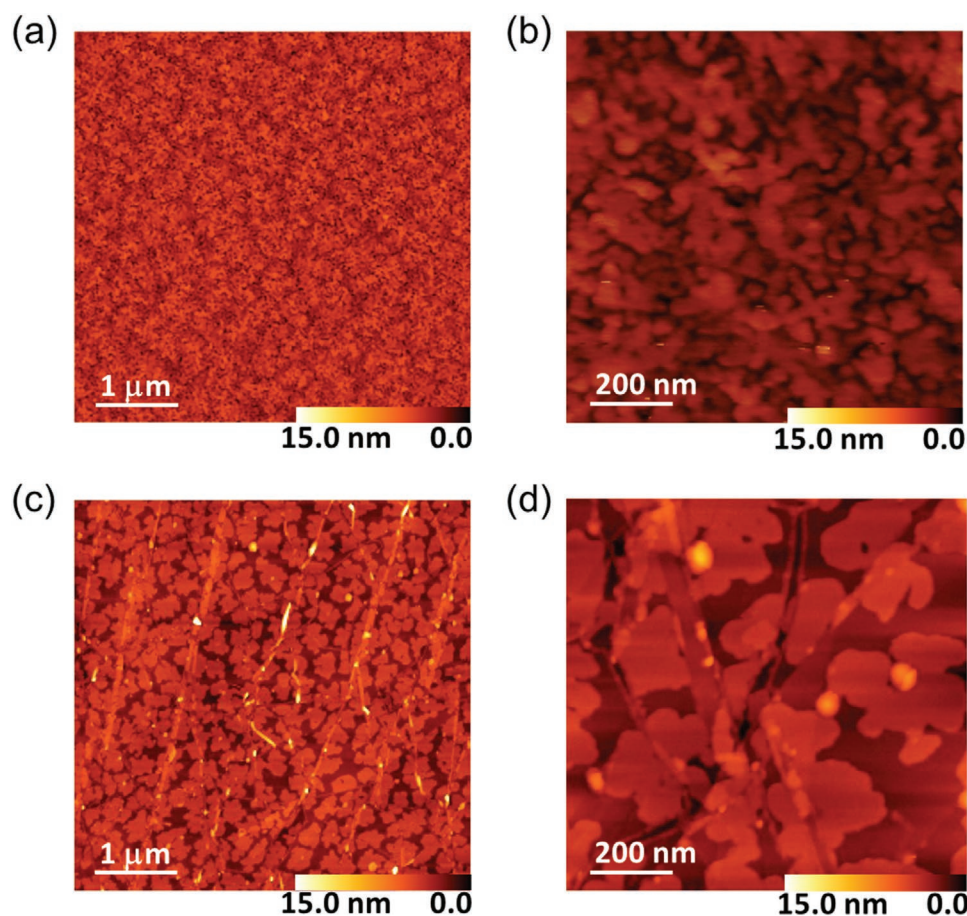
2. Results

2.1. Pristine WS$_2$ Monolayer on Sapphire and HOPG

The optical microscope images in Figure 1a,1d reveals that our CVD (see schematic in Figure S1, Supporting Information) grown ML-WS$_2$ films provide for sufficient lateral charge carrier percolation paths with the substrate coverage typically greater than 90%. Few bright spots on sapphire and dark spots on HOPG, respectively, correspond to WS$_2$ multilayers present at growth nucleation sites. The contrast reversal of these sites in optical microscopy is due to the different optical properties of the substrates, that is, transparent sapphire and high-opacity HOPG. Multilayers comprise less than 2% of the surface area and therefore provide a negligible contribution to the photoemission spectra reported here (averaging over 1–2 mm^2).

The secondary electron cutoff (SECO) and ARUPS spectra of ML-WS$_2$ on sapphire and HOPG are shown in Figure 1b,1c, and Figure 1e,1f, respectively. From the SECO spectra, we determine the work function (Φ) of pristine ML-WS$_2$ on sapphire to be 4.28 eV and on HOPG as 4.45 eV. The energy distribution curves (EDCs) measured at different take-off angles indicate

that the valence band exhibits the energy versus momentum [E(k)] dispersion expected for ML-TMDC films consisting of azimuthally randomly oriented flakes, that is, due to angular averaging the photoemission spectra consist of a superposition of the k-DOS along the Γ-K and Γ-M directions.[35] One local VBM is observed at the Γ-point of the BZ and the global VBM at the K-point. The valence band onset at the K-point is 1.75 eV below the Fermi level (E_F) on sapphire, and 1.42 eV below E_F on HOPG. On both substrates, ML-WS$_2$ thus exhibits n-type behavior, which is more pronounced on sapphire. This is most likely due to native sulfur-vacancies, whose electron donor character has been invoked from experiments[42] and theory.[43]

In the present samples, the S-vacancy induced gap state density is too low to be unambiguously observed within the limits of the dynamic range of the used setup. The valence spectrum recorded at the K-point and plotted on a logarithmic intensity scale (see Figure S2, Supporting Information) gives a vague indication of such gap states just below E_F. For ML-MoS$_2$ corresponding gap states just below E_F have been clearly observed on sapphire substrates, but not with HOPG as support.[31] In analogy to this report, we suggest that also for ML-WS$_2$ (part of) the S-vacancy induced gap states ionize towards the HOPG substrate, rendering the ML less n-type on the conductive substrate compared to the insulating one. From Φ and the VBM onset at K we compute the ML-WS$_2$ ionization energy (IE) to be 6.03 eV on sapphire and 5.87 eV on HOPG. The latter value has a larger error margin because the surface patches not covered by ML-WS$_2$ (i.e., bare HOPG, typically < 10%, vide supra) contribute to the area-average Φ.[49] It is also apparent that the ML-WS$_2$ on HOPG exhibits a narrower valence band peak at and near Γ. This could possibly relate to strain removal during the wet-transfer process[50] from the growth-substrate sapphire to HOPG, and higher areal electrostatic homogeneity of the conductive substrate. For both substrates, the observation of the global VBM at the K-point confirms the predominant contribution of ML surface area to the spectra, because the VBM is located at the Γ-point for multilayers.[51] These findings are in line with the absorption and photoluminescence measured for ML-WS$_2$/sapphire, as shown in Figure S3, Supporting Information. From these spectra, we find an optical gap (lowest exciton energy) of 2.0 eV as expected for the ML-WS$_2$. To estimate the conduction band minimum (CBM) energy above E_F at the K-point, one can add the exciton binding energy to the optical gap yielding the electronic (single particle) bandgap. The exciton binding energy reported for ML-WS$_2$ ranges from 0.71 eV to 0.28 eV.[52–55] The higher values were determined with silicon oxide substrates and the lower one on sapphire, but all employing optical spectroscopy methods only. For the related TMDCs MoS$_2$ and WSe$_2$, the exciton binding energy was obtained by direct measurements of the optical and single particle gaps with sapphire as substrate, amounting to 0.24 eV.[36] Due to the direct determination used in the latter report, we use this value in the following as a lower boundary. Accordingly, we set the electronic gap of ML-WS$_2$/sapphire to 2.24 eV and position the global CBM 0.49 eV above E_F. Because sapphire and HOPG have similar dielectric constants of ca. 10,[40,41] we can reasonably assume a comparable electronic bandgap also on HOPG, which places the CBM for ML-WS$_2$/HOPG ca. 0.82 eV above E_F.

**ADVANCED
SCIENCE NEWS**

www.advancedsciencenews.com

**ADVANCED
ELECTRONIC
MATERIALS**

www.advelectronicmat.de

Figure 2. AFM topography micrographs with different magnification of ca. ML C_{60} (nominal thickness: 1 nm) deposited on a,b) WS_2/sapphire and c,d) WS_2/HOPG. The RMS roughness values of the shown areas are: (a) 1.0, (b) 1.0, (c) 1.1, and (d) 1.0 nm.

2.2. C_{60}/ML-WS_2 on Sapphire and HOPG

The morphology of a nominally 1 nm thick C_{60} film, ca. ML, deposited on ML-WS_2/sapphire and on ML-WS2/HOPG is compared in **Figure 2**. The atomic force microscopy (AFM) images exhibit a rather smooth C_{60} morphology in both cases, with root-mean-square (RMS) roughness values of ca. 1 nm on the shown areas. The images, particularly those with higher magnification, reveal that the C_{60} ML is not fully closed. On ML-WS_2/sapphire, C_{60} features rather small islands with local corrugation between them of ca. 1 nm, corresponding to the C_{60} molecular diameter (Figure 2b). On ML-WS_2/HOPG, the apparent individual C_{60} islands are larger (Figure 2d). In both cases, C_{60} covers the WS_2 surfaces quite well, and the smaller island size with insulating sapphire as supporting substrate may be due to a laterally more corrugated electrostatic potential landscape, compared to a smoother one on the conductive HOPG. The presence of high-quality C_{60} layers on ML-WS_2 is a prerequisite for reliable assessment of the interfacial electronic properties when supported by different substrates.

For ARUPS and XPS measurements, C_{60} was deposited with incremental thickness onto ML-WS_2, and characterized after each deposition step without breaking ultrahigh vacuum (UHV) conditions. **Figure 3** shows the corresponding ARUPS spectra

recorded at the Γ- and K-point of the BZ. At Γ, with a local VBM of ML-WS_2, the WS_2 features exhibit the strongest signal, helping to track possible energy shifts of the WS_2 valence band upon C_{60} deposition more precisely. At K, with the global VBM, the most relevant energy offset between the frontier energy levels of the two materials can be readily determined. The SECO spectra in Figure 3a,3d reveals constant Φ values of 4.28 (sapphire) and 4.45 eV (HOPG) for C_{60} up to 2 nm coverage on both substrates, implying that vacuum level alignment prevails. This is synonymous with negligible electron density rearrangement upon interface formation and thus the absence of any significant electron transfer to C_{60} in both cases. This is in contrast to what was observed at the interface between the fluorinated fullerene $C_{60}F_{48}$ and ML-WS_2/HOPG,[48] and is in line with the significantly larger electron affinity (EA) of $C_{60}F_{48}$ of ca. 5.0 eV[56] compared to that of C_{60} of only ca. 4.0 eV.[57] As displayed in Figure 3b,3e, upon C_{60} deposition the ARUPS spectra taken at the Γ-point for both substrates show an increasing intensity on the high binding energy side of the sharp WS_2 peak. This emission can readily be attributed to stem from the C_{60} highest occupied molecular orbital (HOMO) level. When the thickness of C_{60} goes beyond 1 nm, further deposition of molecules leads to reduced spectral intensity from WS_2, which cannot further be discerned at 2 nm-C_{60} coverage. These results
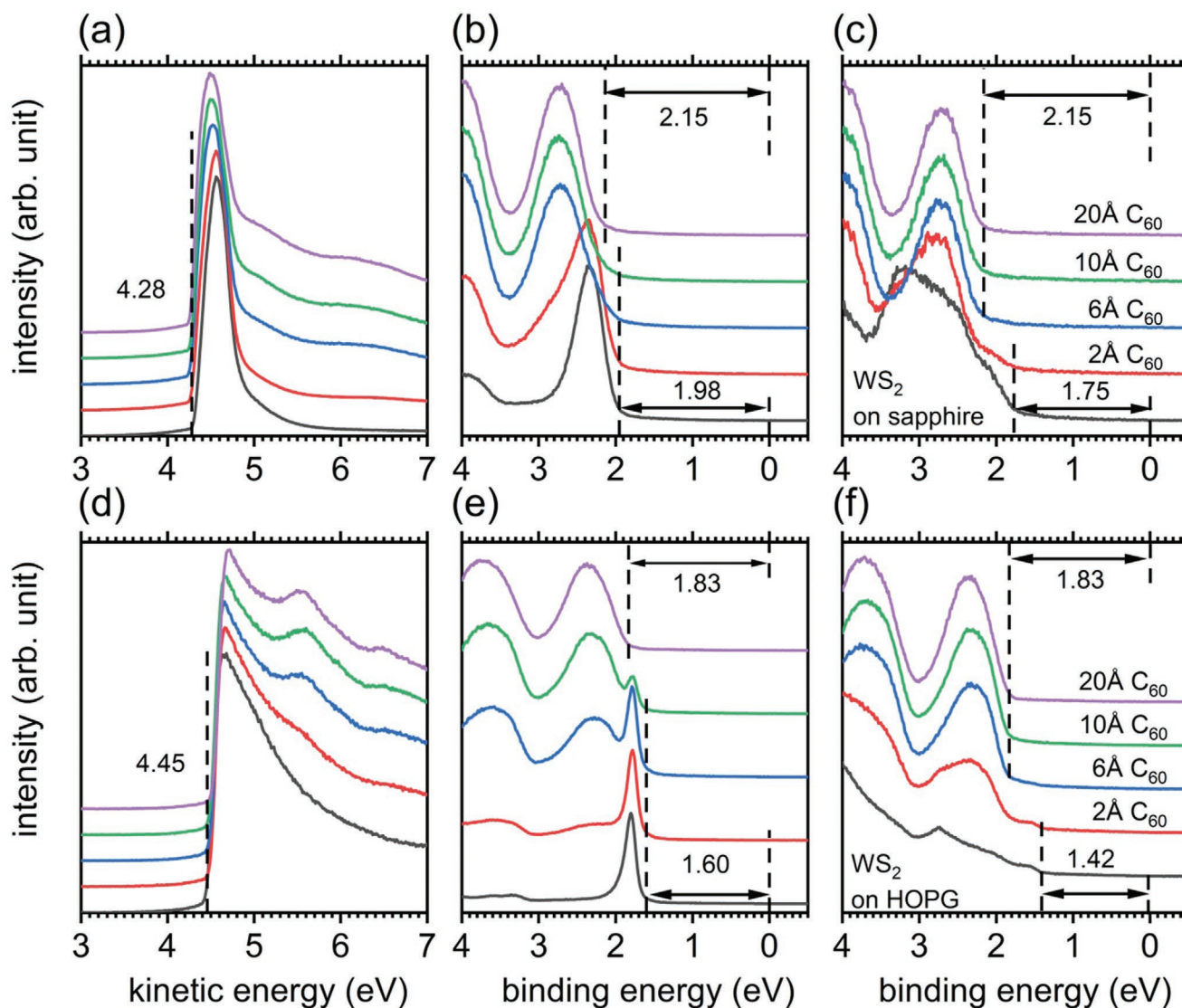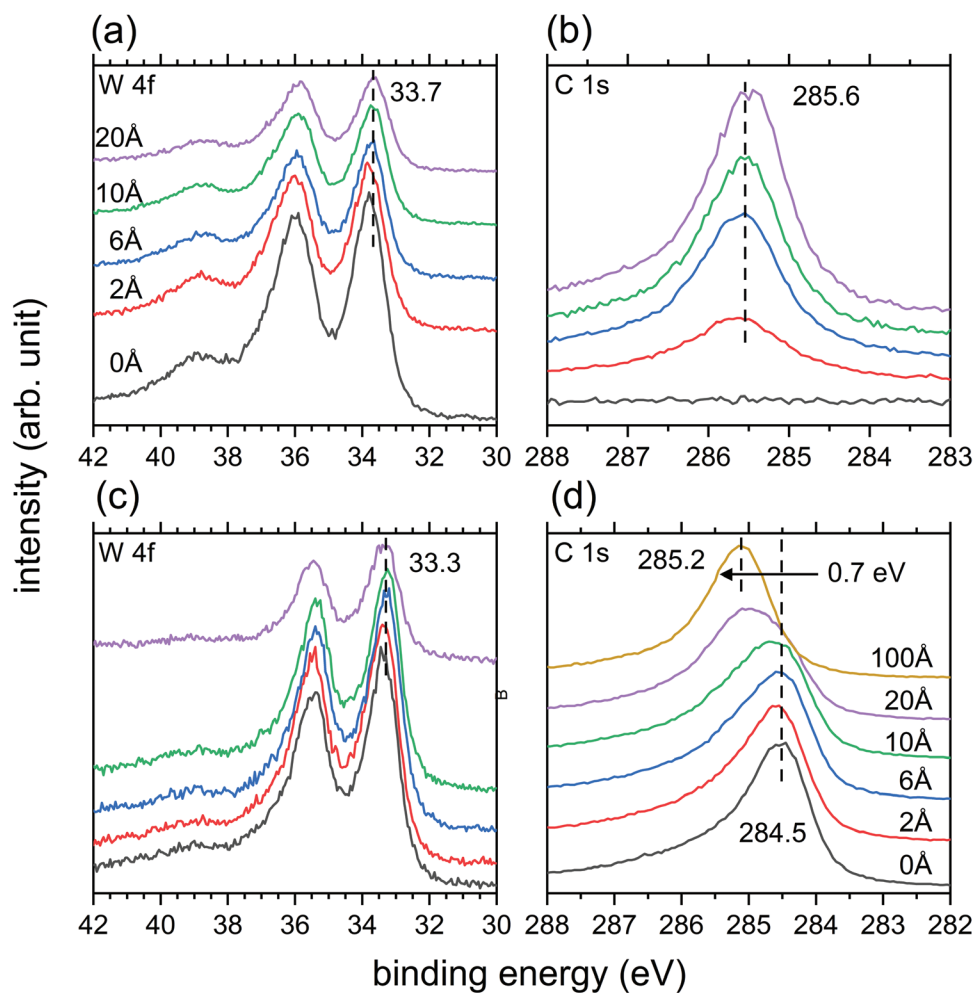
Figure 3. ARUPS spectra of ML-WS$_2$/substrate (sapphire: top row; HOPG: bottom row) with increasing C$_{60}$ coverage, as indicated. a,d) SECO region. b,e) Valence region at the Γ point and c,f) at the K/M points of the BZ. The intensity is normalized for better clarity.

are from the short photoelectron mean free path (< 1 nm) at the kinetic energies in the experiment, and further suggest layered growth of C$_{60}$ on WS$_2$ beyond the ML. The sharp ML-WS$_2$ peak at the Γ-point remains at constant binding energy (particularly clearly seen up to 1 nm C$_{60}$ coverage for the HOPG substrate). This strongly suggests that the local VBM energy position is also constant for both studied systems.

From Figure 3b,3e, we further determine a constant C$_{60}$ HOMO level onset at 2.15 (sapphire) and 1.83 eV (HOPG) binding energy throughout the investigated thickness range. The valence spectra recorded at the K-point of the BZ (Figure 3c,3f) exhibit fully analogous behavior. However, a clear signal from ML-WS$_2$ is observed only up 0.6 nm C$_{60}$ coverage. Additional support for unchanged ML-WS$_2$ energy levels also for thicker C$_{60}$ layers comes from inspection of spectra where the (intensity-scaled) contribution of bare ML-WS$_2$ was subtracted from the measured spectra, shown in Figure S4,

Supporting Information. The residuals are clear replicas of the C$_{60}$ valence features, without any apparent energy shift or shape-change. With this, we can directly assess the energy difference between global VBM at the K-point and the C$_{60}$ HOMO level onset, which amounts to 0.39–0.40 eV for both substrates, sapphire and HOPG.

We finally attend to the W 4f and C 1s core-level spectra from XPS for C$_{60}$/ML-WS$_2$ (shown in **Figure 4**), to further evaluate interfacial interactions on the different supporting substrates. For the heterostructure on sapphire, we observe no apparent changes in the shape of the W 4f and C 1s levels upon deposition of C$_{60}$. However, fitting of the W 4f$_{7/2}$ peak maximum could suggest an incremental shift by up to ca. 0.1 eV to lower binding energy as the C$_{60}$ coverage increases to 2 nm. In contrast, the C 1s remains at a constant energy. A similar shift of the W 4f$_{7/2}$ peak maximum by ca. 0.1 eV towards lower binding energy is also found for the heterostructure on HOPG, however,

**ADVANCED
SCIENCE NEWS**

www.advancedsciencenews.com

**ADVANCED
ELECTRONIC
MATERIALS**

www.advelectronicmat.de

Figure 4. Core level spectra of ML-WS$_2$/substrate (sapphire: top row; HOPG: bottom row) with increasing C$_{60}$ coverage as indicated. a,c) W 4f region. b,d) C 1s region.

with large scatter. With the data at hand, solid evidence for a systematic shift of the W 4f core level cannot be derived, and a detailed further study is needed to investigate this issue on general grounds. For instance, the additional dielectric screening of the photo-holes in WS$_2$ by the C$_{60}$ overlayer may be responsible for such shifts towards lower binding energy. It would also be interesting in this context to compare if screening-induced shifts of core levels and valence levels are quantitatively the same. Our present valence region data suggest no C$_{60}$-induced binding energy shifts of the frontier levels, but we are limited to C$_{60}$ nominal coverages up to 1 nm, beyond which no signal from WS$_2$ can be detected due to the high surface-sensitivity of ARUPS with He I excitation as used here. To investigate WS$_2$ under thicker overlayers, the use of much lower photon energy, and thus longer electron inelastic mean free path, would be required.

In addition, the W 4f levels on HOPG are shifted by ca. 0.4 eV towards lower binding energy compared to those on the sapphire substrate. Since the valence levels of ML-WS$_2$ on both substrates are also shifted by the same amount, this supports the notion of an electrostatic origin of the shift, most likely indeed rooted in the transfer of ML-WS$_2$ gap state density

towards HOPG and the apparent reduced n-type character (vide supra). In contrast, the C 1s peak in Figure 4d seems to gradually shift upon C$_{60}$ deposition. But here we already start with the carbon signal from the HOPG substrate, at ca. 284.5 eV binding energy. As shown in Figure S5, Supporting Information, the addition of a second C 1s component fixed at 0.7 eV higher binding energy (i.e., 285.2 eV) is sufficient to adequately fit all spectra with intermediate C$_{60}$ coverage. Thus, this second C 1s component can be assigned to stem from C$_{60}$, and we conclude on the constant shape and binding energy, again in full consistency with the ARUPS results.

2.3. Interfacial Energy Level Diagrams

Having accessed the alignment of the occupied energy levels of C$_{60}$/ML-WS$_2$ on both substrates above, we now turn towards describing the full interfacial energy level diagrams. The IE of ML-WS$_2$ was determined by adding the global VBM onset binding energy to the sample Φ, resulting in 6.03 (on sapphire) and 5.87 eV (on HOPG). The corresponding EA values are estimated by subtracting the bandgap of 2.24 eV (see discussion
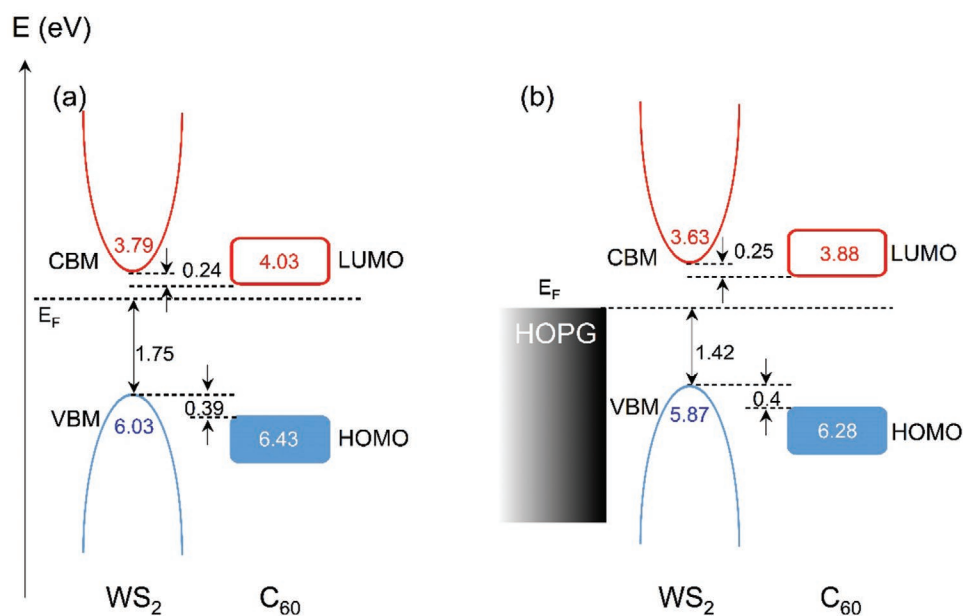
Figure 5. Schematic energy level diagrams for a) C_{60}/ML-WS$_2$/sapphire and b) C_{60}/ML-WS$_2$/HOPG. The blue and red lines depict the occupied and unoccupied levels, respectively. All values are given in eV, the EA and IE values with respect to the vacuum level, set to zero.

above) from the IE, yielding 3.79 (sapphire) and 3.63 eV (HOPG). In analogy, the IE of the C_{60} layers atop ML-WS$_2$ is obtained by adding the binding energy of the HOMO level onset to Φ, giving 6.43 (on sapphire) and 6.28 eV (on HOPG). The C_{60} electronic gap was reported to be 2.3 eV,[58] and more recently reassessed to be 2.4 eV,[59] so that we obtain EA values of 4.03 (sapphire) and 3.88 eV (HOPG). The small difference in the measured IE (and estimated EA) of C_{60} on the two substrates might be due to variations of film morphology, as already ca. ML C_{60} exhibits different morphology (see Figure 2). The observations in a previous study could suggest that smoother C_{60} morphology results in lower IE.[60] All energy levels and the measured position of E_F are summarized in **Figure 5** for both substrates. For both studied structures, the formation of a type-II heterojunction with C_{60} acting as the electron acceptor component is observed, in qualitative agreement with recently reported theoretical modeling data.[13] Notably, the energy offset between the two components' frontier energy levels is nearly identical on both supporting substrates, with 0.4 eV for holes and 0.25 eV for electrons. This is due to the fact that both interfaces exhibited vacuum level alignment, that is, negligible charge density reorganization upon contact. Furthermore, this observation confirms the assumption that the level alignment is the same for an insulating and a conductive substrate, provided that their dielectric constants are rather similar, as is the case for sapphire and HOPG. In contrast, the position of E_F with respect to the electronic levels differs by 0.33 eV for the two substrates. We ascribed the more n-type character of the heterostructure on the sapphire substrate to native, sulfur-vacancy-induced, donor-type gap states close to E_F, which are deactivated by transfer of these electrons towards the charge reservoir offered by HOPG.

At first glance, the C_{60}/ML-WS$_2$ interface is expected to enable efficient charge separation after optical excitation of

either component, which could be used in photodetectors or photovoltaic applications. However, we recall that ML-WS$_2$ is an excitonic semiconductor, with the energy of the first optical transition—forming the exciton—being at least 0.24 eV lower in energy than the bandgap. Looking at Figure 5, we realize that the energy offset between the single-particle unoccupied levels (global CBM and LUMO) has the same magnitude as the WS$_2$ exciton binding energy, so that interfacial charge transfer might actually require excitation with an energy larger than the first exciton of the inorganic semiconductor ML.

3. Conclusions

We studied the electronic properties of a prototypical heterostructure formed by a molecular semiconductor (C_{60}) and a 2D inorganic semiconductor (ML-WS$_2$), on two different supporting substrates. Independent of whether the substrate is insulating (sapphire) or conductive (HOPG), no indication of ground-state charge transfer upon interface formation was found, that is, vacuum level alignment prevailed. The energy offsets between the occupied and unoccupied frontier electronic levels of C_{60} and ML-WS$_2$ were found to be almost identical for both substrates, because the average dielectric constants of sapphire and HOPG are very similar, thus not leading to a substrate-dependent bandgap renormalization of ML-WS$_2$. In contrast, the position of E_F with respect to the energy levels depended on the substrate, with a more pronounced n-type character on sapphire. We suggest that native donor-type levels close to the conduction band, induced by sulfur-vacancies, bestow ML-WS$_2$/sapphire with the apparent n-type character. These gap states are (partially) emptied into the charge reservoir of the conductive HOPG substrate and ML-WS$_2$ exhibits more intrinsic character. Overall, the C_{60}/ML-WS$_2$ interface is

characterized by a type-II level alignment, with C_{60} acting as an electron acceptor, which makes this heterostructure interesting for further investigations in photo-responsive device structures. However, the energy level offset between the global CBM of ML-WS_2 and the C_{60} LUMO is virtually equal to the exciton binding energy of the inorganic ML, thus efficient electron transfer after optical excitation may only occur for excitation energies higher than the ML-WS_2 fundamental exciton.

4. Experimental Section

Synthesis of Monolayer WS_2 Flakes and High-Coverage Monolayer Films: The WS_2 growth was performed in a tube furnace as schematically illustrated in Figure S1, Supporting Information. 30 mg of WO_3 (Sigma-Aldrich, 99.995%) powder was placed in an alumina crucible in the heating zone of the furnace. A sapphire substrate, which was consecutively cleaned by piranha solution, deionized (DI) water, and acetone/isopropanol for half an hour, respectively, and annealed for 1 h at 1000 °C in air, was placed right above the WO_3 powder. 2 g sulfur (Sigma-Aldrich, 99,998%) was introduced in a separate quartz boat at the upstream maintained at 200 °C during the reaction. The tube was first evacuated with a rotary pump to 10^{-2} mbar, and then refilled with Ar till atmospheric pressure. During the reaction, the center zone of the furnace was heated to 900 °C with a constant Ar gas flow (flow rate of 50 sccm) and maintained for 20 min.

WS_2 Monolayer Film Transfer Process: The as-grown ML-WS_2 was transferred from the sapphire onto a HOPG substrate with the commonly used wet-transfer method.[61] A layer of poly (methyl methacrylate) (PMMA) was spin-coated onto the WS_2 and acted as a supporting layer. Hot base (KOH) was then used as a substrate etchant to lift off the PMMA/WS_2 film, after which the PMMA/WS_2 film was cleaned in DI water and transferred to the HOPG substrate. The transferred sample was finally soaked in acetone for 30 min to remove PMMA.

Deposition of C_{60} Films: C_{60} powder (Sigma-Aldrich, purity >99.9%) was evaporated from a resistively heated alumina crucible which was enclosed in an evaporation chamber with a pressure in the 10^{-8} mbar range. The nominal film thickness was determined using a quartz crystal microbalance, using a mass density of 1.65 g cm^{-3}. Correspondingly, the given nominal film thickness values are based on the deposited mass per unit area.

Characterization of the Heterostructures using Atomic Force Microscopy: AFM topography measurements were performed in peak force tapping mode by using a Bruker Icon AFM and ScanasystAir cantilevers in ambient air with a typical resonance frequency of 70 kHz and spring constant of 0.4 N m^{-1}.

Characterization of the Heterostructures using Photoluminescence (PL): PL measurements were conducted with a confocal microscope (XploRA, Horiba Ltd.) using a 532 nm (2.33 eV) laser. The laser was focused by a 100 × objective to a spot size of about 1 µm. The excitation power was maintained lower than 150 µW for PL measurements to avoid nonlinear optical effects and ablation. All measurements were conducted in ambient conditions at room temperature.

Characterization of the Heterostructures using Sample Preparation: Prior to photoemission measurements, the ML WS_2/sapphire and WS_2/HOPG samples were annealed in situ overnight at 350 °C in an UHV preparation chamber with a base pressure of 10^{-9} mbar to remove carbon contaminations.

Characterization of the Heterostructures using C_{60} deposition: The C_{60} molecules were deposited from a resistively annealed crucible at a pressure in the 10^{-9} mbar range and the nominal film thickness was estimated using a quartz microbalance and a density of 1.65 g cm^{-3}.

Characterization of the Heterostructures using Photoemission Spectroscopy: ARUPS and XPS spectra were measured in situ in a UHV chamber (base pressure 2×10^{-10} mbar) with a hemispherical electron analyzer (SPECS Phoibos 100). All shown ARUPS measurements were

performed with the He Iα radiation (21.22 eV) from a monochromated helium discharge lamp (FOCUS HIS-13 Mono) and using an overall energy resolution of ca. 130 meV as determined from the Fermi edge of a polycrystalline gold sample and an angular resolution of ca. ± 4 degrees. XPS measurements were performed with the Mg Kα radiation (1253.6 eV) of a non-monochromated dual anode X-ray source (SPECS XR 50) and using an energy resolution of ca. 1.1 eV as determined from the full-width half-maximum of the Ag 3d of a polycrystalline silver sample. The error of the given Φ, IE, and EA values was estimated to be ± 50 meV. The Φ values were determined from the SECO spectra, measured with −10 V sample bias. For the sapphire substrate, proper WS_2 ML electrical grounding was established by contacting all sample edges with metal clips (connected to the metal sample holder), to prevent charging during the photoemission measurement. Proper grounding of the ML-WS_2 layer on sapphire substrates, that is, the absence of sample charging, was confirmed by observation of a constant binding energy of ML-WS_2 spectral features (core levels in XPS and valence bands in ARUPS) upon varying the excitation photon flux by over one order of magnitude. Furthermore, all spectral features did not exhibit changes in broadening for varied photon fluxes. For HOPG substrates, the WS_2 ML was connected to the ground through the conductive substrates.

Conflict of Interest

The authors declare no conflict of interest.

Data Availability Statement

The data that support the findings of this study are available from the corresponding author upon reasonable request.

[1] K. F. Mak, J. Shan, *Nat. Photonics* **2016**, *10*, 216.
[2] Z. Sun, A. Martinez, F. Wang, *Nat. Photonics* **2016**, *10*, 227.
[3] M. Osada, T. Sasaki, *Adv. Mater.* **2012**, *24*, 210.
[4] M. S. Choi, G.-H. Lee, Y.-J. Yu, D.-Y. Lee, S. H. Lee, P. Kim, J. Hone, W. J. Yoo, *Nat. Commun.* **2013**, *4*, 1624.
[5] B. Radisavljevic, A. Radenovic, J. Brivio, V. Giacometti, A. Kis, *Nat. Nanotechnol.* **2011**, *6*, 147.

[6] D. J. Late, B. Liu, H. R. Matte, V. P. Dravid, C. Rao, *ACS Nano* **2012**, *6*, 5635.

[7] L. Britnell, R. Gorbachev, R. Jalil, B. Belle, F. Schedin, A. Mishchenko, T. Georgiou, M. Katsnelson, L. Eaves, S. Morozov, *Science* **2012**, *335*, 947.

[8] D. J. Late, Y.-K. Huang, B. Liu, J. Acharya, S. N. Shirodkar, J. Luo, A. Yan, D. Charles, U. V. Waghmare, V. P. Dravid, *ACS Nano* **2013**, *7*, 4879.

[9] Z. Yin, H. Li, H. Li, L. Jiang, Y. Shi, Y. Sun, G. Lu, Q. Zhang, X. Chen, H. Zhang, *ACS Nano* **2012**, *6*, 74.

[10] H. S. Lee, S.-W. Min, Y.-G. Chang, M. K. Park, T. Nam, H. Kim, J. H. Kim, S. Ryu, S. Im, *Nano Lett.* **2012**, *12*, 3695.

[11] M. Bernardi, M. Palummo, J. C. Grossman, *Nano Lett.* **2013**, *13*, 3664.

[12] M.-L. Tsai, S.-H. Su, J.-K. Chang, D.-S. Tsai, C.-H. Chen, C.-I. Wu, L.-J. Li, L.-J. Chen, J.-H. He, *ACS Nano* **2014**, *8*, 8317.

[13] L.-Y. Gan, Q. Zhang, Y. Cheng, U. Schwingenschlögl, *J. Phys. Chem. Lett.* **2014**, *5*, 1445.

[14] A. K. Geim, *Science* **2009**, *324*, 1530.

[15] S. J. McDonnell, R. M. Wallace, *Thin Solid Films* **2016**, *616*, 482.

[16] Q. H. Wang, K. Kalantar-Zadeh, A. Kis, J. N. Coleman, M. S. Strano, *Nat. Nanotechnol.* **2012**, *7*, 699.

[17] G. Fiori, F. Bonaccorso, G. Iannaccone, T. Palacios, D. Neumaier, A. Seabaugh, S. K. Banerjee, L. Colombo, *Nat. Nanotechnol.* **2014**, *9*, 768.

[18] F. H. Koppens, T. Mueller, P. Avouris, A. C. Ferrari, M. S. Vitiello, M. Polini, *Nat. Nanotechnol.* **2014**, *9*, 780.

[19] Y. Ma, Y. Dai, M. Guo, C. Niu, J. Lu, B. Huang, *Phys. Chem. Chem. Phys.* **2011**, *13*, 15546.

[20] H. Zhang, L.-M. Liu, W.-M. Lau, *J. Mater. Chem. A* **2013**, *1*, 10821.

[21] Y. Ye, J. Xiao, H. Wang, Z. Ye, H. Zhu, M. Zhao, Y. Wang, J. Zhao, X. Yin, X. Zhang, *Nat. Nanotechnol.* **2016**, *11*, 598.

[22] K. F. Mak, C. Lee, J. Hone, J. Shan, T. F. Heinz, *Phys. Rev. Lett.* **2010**, *105*, 136805.

[23] W. S. Yun, S. Han, S. C. Hong, I. G. Kim, J. Lee, *Phys. Rev. B* **2012**, *85*, 033305.

[24] B. Zhu, X. Chen, X. Cui, *Sci. Rep.* **2015**, *5*, 9218.

[25] D. Jariwala, T. J. Marks, M. C. Hersam, *Nat. Mater.* **2017**, *16*, 170.

[26] D. Jariwala, S. L. Howell, K. S. Chen, J. Kang, V. K. Sangwan, S. A. Filippone, R. Turrisi, T. J. Marks, L. J. Lauhon, M. C. Hersam, *Nano Lett.* **2016**, *16*, 497.

[27] F. Liu, W. L. Chow, X. He, P. Hu, S. Zheng, X. Wang, J. Zhou, Q. Fu, W. Fu, P. Yu, *Adv. Funct. Mater.* **2015**, *25*, 5865.

[28] D. Jariwala, A. R. Davoyan, J. Wong, H. A. Atwater, *ACS Photonics* **2017**, *4*, 2962.

[29] J.-K. Kim, K. Cho, T.-Y. Kim, J. Pak, J. Jang, Y. Song, Y. Kim, B. Y. Choi, S. Chung, W.-K. Hong, *Sci. Rep.* **2016**, *6*, 36775.

[30] M. Gobbi, E. Orgiu, P. Samorì, *Adv. Mater.* **2018**, *30*, 1706103.

[31] S. Park, T. Schultz, X. Xu, B. Wegner, A. Aljarb, A. Han, L.-J. Li, V. C. Tung, P. Amsalem, N. Koch, *Commun. Phys.* **2019**, *2*, 109.

[32] A. Raja, A. Chaves, J. Yu, G. Arefe, H. M. Hill, A. F. Rigosi, T. C. Berkelbach, P. Nagler, C. Schüller, T. Korn, *Nat. Commun.* **2017**, *8*, 15251.

[33] M. Florian, M. Hartmann, A. Steinhoff, J. Klein, A. W. Holleitner, J. J. Finley, T. O. Wehling, M. Kaniber, C. Gies, *Nano Lett.* **2018**, *18*, 2725.

[34] M. Drueppel, T. Deilmann, P. Krueger, M. Rohlfing, *Nat. Commun.* **2017**, *8*, 2117.

[35] S. Park, T. Schultz, X. Xu, B. Wegner, A. Aljarb, A. Han, L.-J. Li, V. C. Tung, P. Amsalem, N. Koch, *Commun. Phys.* **2019**, *2*, 109.

[36] S. Park, N. Mutz, T. Schultz, S. Blumstengel, A. Han, A. Aljarb, L.-J. Li, E. J. List-Kratochvil, P. Amsalem, N. Koch, *2D Mater.* **2018**, *5*, 025003.

[37] A. Vollmer, X. Feng, X. Wang, L. Zhi, K. Müllen, N. Koch, J. Rabe, *Appl. Phys. A* **2009**, *94*, 1.

[38] Y. Xuan, Y. Wu, T. Shen, M. Qi, M. A. Capano, J. A. Cooper, P. Ye, *Appl. Phys. Lett.* **2008**, *92*, 013101.

[39] M. Burghard, H. Klauk, K. Kern, *Adv. Mater.* **2009**, *21*, 2586.

[40] J. Fontanella, C. Andeen, D. Schuele, *J. Appl. Phys.* **1974**, *45*, 2852.

[41] R. J. Papoular, R. Papoular, *Mon. Not. R. Astron. Soc.* **2014**, *443*, 2974.

[42] S.-S. Chee, C. Oh, M. Son, G.-C. Son, H. Jang, T. J. Yoo, S. Lee, W. Lee, J. Y. Hwang, H. Choi, *Nanoscale* **2017**, *9*, 9333.

[43] S. Salehi, A. Saffarzadeh, *Surf. Sci.* **2016**, *651*, 215.

[44] D. M. Guldi, M. Prato, *Acc. Chem. Res.* **2000**, *33*, 695.

[45] P. W. Blom, V. D. Mihailetchi, L. J. A. Koster, D. E. Markov, *Adv. Mater.* **2007**, *19*, 1551.

[46] M. Remškar, A. Mrzel, A. Jesih, J. Kovač, H. Cohen, R. Sanjinés, F. Lévy, *Adv. Mater.* **2005**, *17*, 911.

[47] R. Chen, C. Lin, H. Yu, Y. Tang, C. Song, L. Yuwen, H. Li, X. Xie, L. Wang, W. Huang, *Chem. Mater.* **2016**, *28*, 4300.

[48] Z. Song, T. Schultz, Z. Ding, B. Lei, C. Han, P. Amsalem, T. Lin, D. Chi, S. L. Wong, Y. J. Zheng, *ACS Nano* **2017**, *11*, 9128.

[49] T. Schultz, T. Lenz, N. Kotadiya, G. Heimel, G. Glasser, R. Berger, P. W. Blom, P. Amsalem, D. M. de Leeuw, N. Koch, *Adv. Mater. Interfaces* **2017**, *4*, 1700324.

[50] X. Xu, T. Schultz, Z. Qin, N. Severin, B. Haas, S. Shen, J. N. Kirchhof, A. Opitz, C. T. Koch, K. Bolotin, *Adv. Mater.* **2018**, *30*, 1803748.

[51] I. Tanabe, M. Gomez, W. C. Coley, D. Le, E. M. Echeverria, G. Stecklein, V. Kandyba, S. K. Balijepalli, V. Klee, A. E. Nguyen, *Appl. Phys. Lett.* **2016**, *108*, 252103.

[52] A. Hanbicki, M. Currie, G. Kioseoglou, A. Friedman, B. Jonker, *Solid State Commun.* **2015**, *203*, 16.

[53] B. Zhu, X. Chen, X. Cui, *Sci. Rep.* **2015**, *5*, 9218.

[54] W.-T. Hsu, J. Quan, C.-Y. Wang, L.-S. Lu, M. Campbell, W.-H. Chang, L.-J. Li, X. Li, C.-K. Shih, *2D Mater.* **2019**, *6*, 025028.

[55] A. Chernikov, T. C. Berkelbach, H. M. Hill, A. Rigosi, Y. Li, O. B. Aslan, D. R. Reichman, M. S. Hybertsen, T. F. Heinz, *Phys. Rev. Lett.* **2014**, *113*, 076802.

[56] M. T. Edmonds, M. Wanke, A. Tadich, H. Vulling, K. J. Rietwyk, P. L. Sharp, C. Stark, Y. Smets, A. Schenk, Q.-H. Wu, *J. Chem. Phys.* **2012**, *136*, 124701.

[57] M. Shibuta, K. Yamamoto, T. Ohta, M. Nakaya, T. Eguchi, A. Nakajima, *Sci. Rep.* **2016**, *6*, 35853.

[58] R. Lof, M. Van Veenendaal, B. Koopmans, H. Jonkman, G. Sawatzky, *Phys. Rev. Lett.* **1992**, *68*, 3924.

[59] H. Yoshida, *J. Phys. Chem. C* **2014**, *118*, 24377.

[60] F. Zhang, A. Vollmer, J. Zhang, Z. Xu, J. Rabe, N. Koch, *Org. Electron.* **2007**, *8*, 606.

[61] J. Kang, D. Shin, S. Bae, B. H. Hong, *Nanoscale* **2012**, *4*, 5527.